Revisiting the recollisional (e, $2e$) process in strong-field nonsequential double ionization of helium

Zhangjin Chen, Yali Wang, and Lina Zhang
Department of Physics, College of Science, Shantou University, Shantou, Guangdong 515063, People's Republic of China

Xiangfu Jia
School of Physics and Information Engineering, Shanxi Normal University, Linfen, Shanxi 041004, People's Republic of China

(Received 21 September 2018; published 4 March 2019)

We present numerical simulations on the correlated two-electron momentum distributions for the recollisional (e, $2e$) process in nonsequential double ionization (NSDI) of helium by an 800-nm laser field at an intensity around $4.5 \times 10^{14}\,\mathrm{W/cm^2}$, based on the improved quantitative rescattering model, in which the lowering of the kinetic energy required for the electrons to escape from the parent ion due to the presence of electric field at the time of recollision has been taken into account. According to the QRS model, the correlated two-electron momentum distributions for laser-induced (e, $2e$) collision in NSDI can be factorized as a product of the returning-electron wave packet (RWP) and the field-free differential cross section (DCS) for ionization of the parent ion by the impact of the laser-induced returning electron. The RWPs which describe the momentum distribution of the returning electrons are obtained within the strong-field approximation for high-order above threshold ionization. In the calculations of the DCSs for electron impact ionization of He^+, the precollision Coulomb interaction between the incident electron and the parent ion and the postcollision Coulomb interaction between the two outgoing electrons are considered. In addition, the dynamic screening (DS) of the three-body Coulomb interactions in the final state, due to the fact that the strength of the interaction of any two particles is affected by the presence of the third one, has also been taken into account. It has been found that while the postcollision Coulomb interaction is responsible for the observed fingerlike structure, the precollision Coulomb interaction changes the orientation of the two fingers from V-type to parallel, the final state DS reduces the separation of the two fingers, and the lowering of threshold energy shifts the two fingers towards smaller momenta. All these effects improve the agreement of the simulated results with the experimental results.

DOI: 10.1103/PhysRevA.99.033401

I. INTRODUCTION

The process of nonsequential double ionization (NSDI) has attracted wide interest both experimentally and theoretically for more than three decades and still remains one of the most fundamental and attractive phenomena in strong-field laser physics because it involves the correlated motion of two electrons. The characteristic knee structure observed in the early experimental measurements of the total double ionization yield as a function of laser intensity [1–4] first unveiled the principal underlying physical mechanisms leading to NSDI. It has now been widely accepted that NSDI can be attributed to two processes, one is the electron impact ionization, in which the first electron, by recolliding with the core, immediately releases a second electron, and the other one is recollision excitation with subsequent ionization. Recently, it has been found that NSDI could also take place through sequential ionization of doubly excited states which are populated after the laser-induced recollision [5,6].

Despite the great stimulation it created, the measured total ionization yield could only give little insight into the ionization mechanism compared to the correlated two-electron momentum distributions which were first measured by Weber *et al.* [7] at the turn of this century. The correlated two-electron momentum distributions have been shown to provide the most detailed information of NSDI since many characteristic structures of that particular process are smoothed out in the momentum distributions and the total yield of the resulting doubly charged ions. Such coincident electron momentum distributions yield direct and intuitive insight into the dynamics of laser-atom interaction and shed light on the mechanism leading to NSDI, and hence serve as a detailed testing ground for various theoretical models.

One decade ago, the prominent fingerlike structure observed in an experiment with high resolution and high statistics on NSDI of helium in a strong laser pulse at 800 nm [8] attracted considerable interest because it provided a particularly clear manner of the electron-electron correlation. A lot of theoretical efforts have been devoted to this special issue. Particularly noteworthy are the *ab inito* calculations by solving the time-dependent Schrödinger equation (TDSE) [8], the semiclassical quasistatic model [9], the classical three-dimensional ensemble model [10], and the quantitative rescattering (QRS) model [11,12]. Due to the high demand of computer resources both in time and in memory, which quickly grows with pulse duration and laser intensity, *ab initio* time-dependent calculations are usually carried out with dimensional restriction as well as a restriction to a few cycles of the laser field. In addition, the dynamical details of the electron recollision process can hardly be extracted from the solution of the TDSE, and hence the transparent physical interpretation of the fingerlike pattern cannot be achieved. Moreover, the semiclassical model allows one to disentangle the physical mechanisms, such as the electron-electron and

electron-ion interactions, and thus identify the influence of each mechanism on the fingerlike structure. However, in the semiclassical model, except for initial tunneling, other physical effects are described classically. In contrast, the QRS model is based on a full quantum formulation, in which all the physical mechanisms are treated quantum mechanically.

The fingerlike structure in the NSDI of helium is attributed to the laser-induced recollisional $(e, 2e)$ process. Although it has been confirmed that the observed fingerlike structure in experiments is a consequence of the Coulomb interaction between the two emitted electrons [9,11,12], obvious discrepancies have been found between the existing theoretical simulations and the experimental data. For example, the separation of the two fingers has always been overestimated [8,9,11,12]. In this paper, we revisit this process by using the improved QRS model [13,14] in which the lowering of the kinetic energy required for the electrons to escape from the parent ion due to the presence of electric field at the instant of recollision has been taken into account. In addition, while both the electron-electron and electron-nucleus interactions in the final state have been included in the numerical simulations, as we did in the previous work [11,12], the influence of the Coulomb interaction between the incident electron and the target-ion on the fingerlike structure is addressed. Furthermore, the dynamic screening effect in the final state three-body system is also examined.

The remainder of the present paper is arranged as follows. The theoretical ingredients and the numerical procedures are presented in Sec. II. The simulated results are shown and discussed in Sec. III. Finally, our conclusions are given in Sec. IV.

Atomic units (a.u.) ($\hbar = |e| = m = 4\pi\epsilon_0 = 1$) are used throughout the paper unless otherwise indicated.

II. THEORETICAL METHODS

According to the QRS model, the correlated two-electron momentum distributions for laser-induced recollision direct ionization can be factorized as a product of the returning-electron wave packet and the field-free differential cross sections for electron impact ionization of the parent ion.

A. Theoretical models for the laser-free $(e, 2e)$ process

Suppose we have an electron with momentum $\boldsymbol{k}_i$ and energy E_i, which collides with a He^+ ion in its ground state; after the collision two electrons, one with momentum $\boldsymbol{k}_1$ and energy E_1, and a second with momentum $\boldsymbol{k}_2$ and energy E_2, are detected in coincidence. For this process, the triple-differential cross section (TDCS) is given by

$$\frac{d^3\sigma}{d\Omega_1 d\Omega_2 dE_2} = (2\pi)^4 \frac{k_1 k_2}{k_i}\left[\frac{3}{4}|f(\boldsymbol{k}_1,\boldsymbol{k}_2) - f(\boldsymbol{k}_2,\boldsymbol{k}_1)|^2 + \frac{1}{4}|f(\boldsymbol{k}_1,\boldsymbol{k}_2) + f(\boldsymbol{k}_2,\boldsymbol{k}_1)|^2\right], \quad (1)$$

where $\Omega_1(\theta_1,\phi_1)$ and $\Omega_2(\theta_2,\phi_2)$ are the solid angles of detectors for the two electrons leaving the collision with momenta $\boldsymbol{k}_1$ and $\boldsymbol{k}_2$, and $f(\boldsymbol{k}_1,\boldsymbol{k}_2)$ and $f(\boldsymbol{k}_2,\boldsymbol{k}_1)$ are the transition amplitudes for the direct and exchange processes, respectively. In the prior form, the direct transition amplitude for the $(e, 2e)$ process is expressed by

$$f(\boldsymbol{k}_1,\boldsymbol{k}_2) = \langle \Psi^-_{\boldsymbol{k}_1,\boldsymbol{k}_2}(\boldsymbol{r}_1,\boldsymbol{r}_2)|V_i|\Psi_{\boldsymbol{k}_i}(\boldsymbol{r}_1,\boldsymbol{r}_2)\rangle, \quad (2)$$

where V_i is the perturbation interaction, and $\boldsymbol{r}_1$ and $\boldsymbol{r}_2$ are the position vectors of the projectile and the bound-state electron, respectively, with respect to the target nucleus.

The final-state wave function, which satisfies the incoming-wave boundary condition, is a solution of the following Schrödinger equation:

$$(H - E_1 - E_2)\Psi^-_{\boldsymbol{k}_1,\boldsymbol{k}_2} = 0, \quad (3)$$

where H is the exact Hamiltonian for the whole system,

$$H = -\frac{1}{2}\nabla_1^2 - \frac{Z_N}{r_1} - \frac{1}{2}\nabla_2^2 - \frac{Z_N}{r_2} + \frac{1}{r_{12}}, \quad (4)$$

with $Z_N = 2$ being the nuclear charge of He. The approximate three-body scattering wave function for the final state that satisfies the asymptotic three-body Schrödinger equation exactly was derived analytically by Brauner, Briggs, and Klar (BBK) [15] and can be expressed as

$$\Psi^-_{\boldsymbol{k}_1,\boldsymbol{k}_2}(\boldsymbol{r}_1,\boldsymbol{r}_2) = (2\pi)^{-3}\exp(i\boldsymbol{k}_1\cdot\boldsymbol{r}_1)\exp(i\boldsymbol{k}_2\cdot\boldsymbol{r}_2) \times C(\alpha_1,\boldsymbol{k}_1,\boldsymbol{r}_1)C(\alpha_2,\boldsymbol{k}_2,\boldsymbol{r}_2)C(\alpha_{12},\boldsymbol{k}_{12},\boldsymbol{r}_{12}), \quad (5)$$

where the Coulomb part of the wave function is defined as

$$C(\alpha,\boldsymbol{k},\boldsymbol{r}) = e^{-\pi\alpha/2}\Gamma(1-i\alpha)\,{}_1F_1[i\alpha;1;-i(kr+\boldsymbol{k}\cdot\boldsymbol{r})], \quad (6)$$

and

$$\boldsymbol{k}_{12} = \frac{1}{2}(\boldsymbol{k}_1 - \boldsymbol{k}_2), \quad \boldsymbol{r}_{12} = \boldsymbol{r}_1 - \boldsymbol{r}_2,$$
$$\alpha_1 = -\frac{Z_N}{k_1}, \quad \alpha_2 = -\frac{Z_N}{k_2}, \quad \alpha_{12} = \frac{1}{2k_{12}}. \quad (7)$$

In Eq. (6), Γ is the Gamma function and ${}_1F_1$ is the confluent hypergeometric function. Since the BBK wave function in Eq. (5) consists of a product of three Coulomb wave functions, it is referred to as 3C, in which the Coulomb interaction between the two outgoing electrons has been taken into account. If $1/r_{12}$ is dropped in Eq. (4), the interaction between the two outgoing electrons is turned off. Consequently, the final-state wave function becomes a product of two Coulomb (2C) wave functions by setting $\alpha_{12} = 0$ in Eq. (5). It should be mentioned that the 2C wave function does not satisfy the proper asymptotic three-body boundary condition.

The initial state $\Psi_{\boldsymbol{k}_i}$ in Eq. (2) can be obtained by solving the following Schrödinger equation:

$$(H_i - E_i - \epsilon_i)\Psi_{\boldsymbol{k}_i}(\boldsymbol{r}_1,\boldsymbol{r}_2) = 0, \quad (8)$$

where ϵ_i is the energy of He^+ in the ground state, and H_i is the approximate Hamiltonian for $(e, 2e)$ processes on He^+ ion in the initial channel and is given by

$$H_i = -\frac{1}{2}\nabla_1^2 - \frac{Z_{\rm eff}}{r_1} - \frac{1}{2}\nabla_2^2 - \frac{Z_N}{r_2}, \quad (9)$$

where $Z_{\rm eff} = Z_N - 1$ is the asymptotic charge of the target seen by the incident electron. With this approximation, the initial state which consists of the incident electron and the bound electron can be expressed as the product of two wave

functions, one describing the incident electron and the second describing the bound electron,

$$\Psi_{\boldsymbol{k}_i}(\boldsymbol{r}_1,\boldsymbol{r}_2)=\varphi_{\boldsymbol{k}_i}(\boldsymbol{r}_1)\phi_{\mathrm{He}^+}(\boldsymbol{r}_2), \tag{10}$$

where $\varphi_{\boldsymbol{k}_i}(\boldsymbol{r}_1)$ describes the incident electron and satisfies

$$\left[-\frac{1}{2}\nabla_1^2-\frac{Z_{\mathrm{eff}}}{r_1}-E_i\right]\varphi_{\boldsymbol{k}_i}(\boldsymbol{r}_1)=0, \tag{11}$$

and $\phi_{\mathrm{He}^+}(\boldsymbol{r}_2)$ is an eigenfunction of the equation

$$\left[-\frac{1}{2}\nabla_2^2-\frac{Z_N}{r_2}-\epsilon_i\right]\phi_{\mathrm{He}^+}(\boldsymbol{r}_2)=0. \tag{12}$$

The eigenfunction of Eq. (11) is a Coulomb wave, which takes the form

$$\varphi_{\boldsymbol{k}_i}(\boldsymbol{r}_1)=\frac{1}{(2\pi)^{3/2}}\exp(-\pi\alpha_i/2)\Gamma(1+i\alpha_i)\times\exp(i\boldsymbol{k}_i\cdot\boldsymbol{r}_1)_1F_1[-i\alpha_i;1;i(k_ir_1-\boldsymbol{k}_i\cdot\boldsymbol{r}_1)], \tag{13}$$

where $\alpha_i=-Z_{\mathrm{eff}}/k_i$. The ground-state wave function of He^+ in Eq. (12) is taken to be

$$\phi_{\mathrm{He}^+}(\boldsymbol{r}_2)=\left(\frac{Z_N^3}{\pi}\right)^{1/2}\exp(-Z_Nr_2). \tag{14}$$

The perturbation interaction in the initial channel is then given by

$$V_i=H-H_i=-\frac{Z_N-Z_{\mathrm{eff}}}{r_1}+\frac{1}{r_{12}}. \tag{15}$$

Due to the long-range Coulomb interaction occurring in the initial channel, further complication arises in the theoretical calculation for the ionization of ions. Alternatively, the incident Coulomb wave is replaced by a plane wave by setting $Z_{\mathrm{eff}}=0$ in Eq. (11), i.e.,

$$\varphi_{\boldsymbol{k}_i}(\boldsymbol{r}_1)=\frac{1}{(2\pi)^{3/2}}\exp(i\boldsymbol{k}_i\cdot\boldsymbol{r}_1). \tag{16}$$

Consequently, the perturbation interaction in the initial channel becomes

$$V_i=-\frac{Z_N}{r_1}+\frac{1}{r_{12}}. \tag{17}$$

It should be noted that in the previous work [11], we chose the perturbation potential in Eq. (17) since only plane waves were used to describe the incident electron. In this paper, we always use the perturbation potential in Eq. (15) since using a plane wave to describe the projectile in the initial channel for the (e, $2e$) process of ions is simply an alternative numerical treatment rather than a reasonable approximation due to the fact that $Z_{\mathrm{eff}}=0$ is never valid.

So far the theoretical models employed in this work can be classified according to the number of Coulomb waves involved in the transition amplitude, which are 2C, 3C, and 4C. In the 2C and 3C models, the incident electron is represented by a plane wave and the two outgoing electrons are represented by a product of two and three Coulomb waves, respectively. In the 4C model, a Coulomb wave is used to describe the incident electron, and a product of three Coulomb waves is employed to represent the two outgoing electrons.

Although the 3C wave function for the two continuum electrons in the final state satisfies the asymptotic three-body Schrödinger equation exactly, it cannot be regarded as fully satisfactory. The major limitation of the 3C wave function lies in the fact that influence on the strength of the interaction of any two particles by the presence of a third one has not been taken into account. This deficiency was first corrected by Berakdar and Briggs [16] by introducing effective Sommerfeld parameters for the case in which the two outgoing electrons have equal energies. Such a modification reflects the dynamic screening (DS) of the three-body Coulomb interactions. This prescription was later generalized by Chen *et al.* [17] for any geometry and energy sharing. In this work, the DS effect has also been considered in the 3C and 4C models, and hence the improved 3C and 4C models are referred to as DS3C and DS4C, respectively. The details of the DS3C model can be found in Refs. [17,18].

B. Numerical procedures for the recollisional (e, $2e$) process in a strong field

For the recollisional (e, $2e$) process of He^+ in a strong field, the first issue one needs to consider is the spin conservation. The TDCS in Eq. (1) is spin averaged for regular (e, $2e$) collisions, in which a spin multiplication factor of 1/4 is included for the singlet cross sections and a factor of 3/4 is included for the triplet cross sections. Equation (1) has been used in our previous calculations for the NSDI of He [11]. However, for the laser-induced recollisional (e, $2e$) process of He^+, the two electrons involved in the process start in the singlet ground state of He, and their singlet coupling is preserved during ionization since the absorption of photons does not affect spin [19]. Thus we need to multiply the singlet scattering cross sections by a factor of 4, and we must neglect the triplet scattering cross sections. Consequently the TDCS for the recollisional (e, $2e$) process of He^+ in a strong field is given by

$$\frac{d^3\sigma_{\mathrm{s}}}{d\Omega_1d\Omega_2dE_2}=(2\pi)^4\frac{k_1k_2}{k_i}|f(\boldsymbol{k}_1,\boldsymbol{k}_2)+f(\boldsymbol{k}_2,\boldsymbol{k}_1)|^2. \tag{18}$$

In the correlated two-electron momentum spectra for NSDI, the experimental data are measured only for the momentum components of the two electrons along the laser polarization axis. Thus, to compare with the experimental data, the TDCS needs to be integrated over the transverse momentum of both the two outgoing electrons. For this purpose, we obtain the two-electron momentum spectra along the incident direction for the laser-free (e, $2e$) process at a given incident energy by integrating the TDCS over ϕ_2 and E_2:

$$Y_{E_i}(k_1^{||},k_2^{||})=\frac{4\pi}{k_1k_2}\int_0^{E_2^{\max}}dE_2\int_0^{\pi}d\phi_2\frac{d^3\sigma_{\mathrm{s}}}{d\Omega_1d\Omega_2dE_2}\bigg|_{\phi_1=0}, \tag{19}$$

where $E_2^{\max}=E_i-I_p$, and I_p is the ionization potential. In the actual calculations, we set $\phi_1=0$ in Eq. (19) owing to the cylindrical symmetry, and the integration over ϕ_2 is performed only from 0 to π since the TDCS is symmetric about the plane formed by $\boldsymbol{k}_1$ and $\boldsymbol{k}_i$.

For the recollisional $(e, 2e)$ process taking place at t_r when the vector potential $\boldsymbol{A}(t_r) = \boldsymbol{A}_r$, the two electrons are still under the influence of the laser field after the collision. As a result, each electron will gain an additional momentum $-A_r$ in the direction of the laser polarization from t_r to the end of laser pulse. Therefore, the corresponding correlated two-electron momentum distribution for the recollisional $(e, 2e)$ process in a strong field at an intensity I can be obtained from Eq. (19) by shifting the momenta of two outgoing electrons using the relation

$$p_j^{||} = k_j^{||} - A_r \quad (j = 1 \text{ and } 2), \tag{20}$$

where $p_1^{||}$ and $p_2^{||}$ are the parallel momenta of the two correlated electrons along the laser polarization, respectively. Consequently, we have

$$D_{E_i,I}(p_1^{||}, p_2^{||}) = Y_{E_i}(k_1^{||} - A_r, k_2^{||} - A_r). \tag{21}$$

Based on the classical simulation [20], for laser-induced elastic scattering which accounts for high-order above-threshold ionization, the vector potential A_r at the collision time is approximately determined by the relation

$$|A_r| = k_r/1.26, \tag{22}$$

where $k_r = k_i$ is the momentum of the returning electron.

However, for laser-induced inelastic scattering, such as electron impact excitation and electron impact ionization of the parent ion in NSDI, the threshold energy could be lowered due to the presence of an electric field [21]. The actual threshold for electron impact ionization of a singly charged ion in an external electric field of strength $F_0 \cos(\omega t_r)$ at the instant of collision is lowered by [14,22]

$$\Delta E = 2\sqrt{2|F_0 \cos(\omega t_r)|}. \tag{23}$$

Nevertheless, it is far from straightforward to perform the actual numerical calculations including the lowering of the threshold. This is partially due to the fact that the barrier height of the combined atomic and electric fields varies with the angle to the polarization axis. Alternatively, we choose an "average" return time of $\bar{t}_r = 290^\circ/\omega$ in our calculations.

The average return time is determined by using the one-dimensional (1D) classical model [23]. Suppose that an electron in the 1D atom is released into a monochromatic laser field, $\boldsymbol{F}(t) = \hat{z}F_0 \cos(\omega t)$, then the Newton's equation of motion for this system is given by

$$\ddot{z}(t) = -F_0 \cos(\omega t). \tag{24}$$

If the electron is initially tunneling ionized with zero initial velocity at the birth time t_b, the return time t_r at which the electron comes back to the origin can be simply identified by solving Eq. (24) [20]. Based on the 1D classical model, it has been found that electrons born before 13° return at a time after 270° and they follow a long trajectory, while those born after 13° return before 270° and they follow a short trajectory. Since the electrons born before 13° have an ionization rate higher than that of those born after 13°, more electrons return to the parent ion after 270°. In Fig. 1, we plot the relative ionization rate against the return time (bottom horizontal axis) as well as the corresponding birth time (top horizontal axis). Here, the ionization rate W_{adk} is calculated

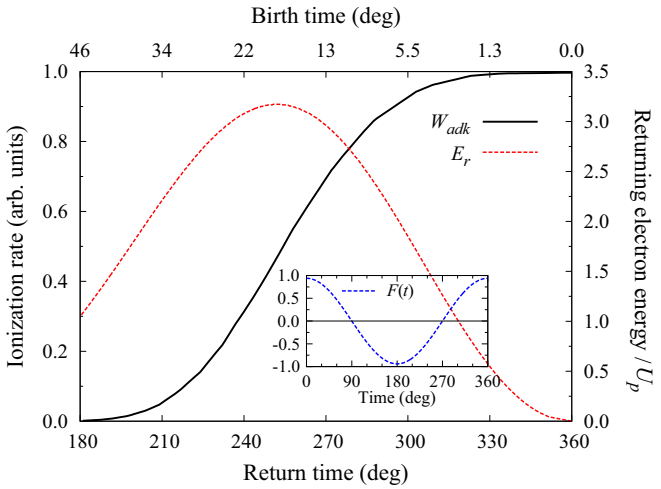

FIG. 1. Relative ionization rate (left vertical axis) and returning-electron energy (right vertical axis) against the return time (bottom horizontal axis) and the corresponding birth time (top horizontal axis). The inset shows the monochromatic laser field used in the 1D classical model. See text for detail.

using the Ammosov-Delone-Krainov (ADK) model [24]. By taking into account the ionization rate at each return time, we can obtain the average return time approximately by

$$\bar{\theta}_r = \frac{\int_{\theta_1}^{\theta_2} \theta_r W_{\text{adk}}(\theta_r) d\theta_r}{\int_{\theta_1}^{\theta_2} W_{\text{adk}}(\theta_r) d\theta_r}, \tag{25}$$

where $\theta_r = \omega t_r$. Furthermore, the returning-electron energy $E_r = k_r^2/2$ can also be obtained from Eq. (24), as shown in Fig. 1 (right vertical axis) in terms of U_p, where U_p is the ponderomotive energy. It can be seen that, with the increase of the return time, the returning-electron energy increases until it reaches the maximum value of $3.17U_p$ at a return time of around $t_r = 252^\circ/\omega$ and then it decreases to $0.5U_p$ at $t_r = 331^\circ/\omega$, corresponding to the photoelectron energy of $2U_p$ in high-order above threshold ionization (HATI). Since direct ionization dominates for photoelectron energy below $2U_p$, we choose $\theta_1 = 180^\circ$ and $\theta_2 = 331^\circ$ for the return time interval in Eq. (25), which gives $\bar{\theta}_r = 288^\circ$. It should be noted that the average return time obtained from Eq. (25) is not very sensitive to the upper limit of the integral. For example, one gets $\bar{\theta}_r = 292^\circ$ for $\theta_2 = 340^\circ$. The validity of this treatment has been verified in our previous work [13,14], in which the improved QRS model has been employed to evaluate the total yield of the doubly charged ion for the NSDI of He and Ne, and the simulated results are in good agreement with experimental dat.

To account for the lowering of the threshold, Eq. (22) should be modified and rewritten as

$$|A_r| = \sqrt{2(E_i - \Delta E)}/1.26. \tag{26}$$

To obtain the correlated two-electron momentum distributions for a given intensity, one has to consider the contributions from collisions at all incident energies such that the

integral over E_i should be performed. This gives

$$D_I(p_1^{||}, p_2^{||}) = \int_{I_p}^{\infty} dE_i D_{E_i,I}(p_1^{||}, p_2^{||}) W_I(E_i - \Delta E), \quad (27)$$

where $W_I(E_i - \Delta E)$ is the returning-electron wave packet [20] in the laser field at a single intensity I, indicating the weight of the contribution at incident energy E_i, which can be calculated by using the improved strong-field approximation for HATI (see Ref. [13] for details). In Eq. (27), the lowering of the threshold has been taken into account by simply adjusting the collision energy [21]. Here, it is assumed that the incident energy with respect to the maximum of the barrier in the combined atomic and electric potential, which is lower than zero, corresponds to the incident energy in the laser-free case. For example, in a laser field at an intensity of 4.5×10^{14} W/cm^2, the threshold is lowered by 15 eV. If the energy of the laser-induced returning electron is 50 eV, the scattering cross sections for the collision taking place in the field correspond to the laser-free scattering cross sections at an incident energy of 65 eV.

Finally, to compare with experimental measurements, the integration over the focus volume should be performed,

$$D_{I_0}(p_1^{||}, p_2^{||}) = \int_0^{I_0} D_I(p_1^{||}, p_2^{||}) \left(\frac{\partial V}{\partial I}\right) dI, \quad (28)$$

where I_0 is the peak intensity of the laser field. This is due to the fact that the intensity distribution of a focused laser beam is not uniform in space, and the atoms located everywhere in the interaction volume experience different peak intensities. For a laser beam with Lorentzian distribution in the propagation direction and Gaussian distribution in the transverse direction, the volume of an isointensity shell between I and $I + dI$ is given by [25]

$$\left(\frac{\partial V}{\partial I}\right) dI = \pi z_R \omega_0^2 \left[\frac{4(c_1 - c_2)}{3} + \frac{2(c_1^3 - c_2^3)}{9} - \frac{4}{3}(\tan^{-1} c_1 - \tan^{-1} c_2)\right], \quad (29)$$

where $2\omega_0$ is the $1/e$ diameter of the focal spot, z_R is the Rayleigh range of the focus, $c_1 = [(I_0 - I)/I]^{1/2}$, and $c_2 = \{[I_0 - (I + dI)]/(I + dI)\}^{1/2}$.

III. RESULTS AND DISCUSSION

We aim to simulate the correlated two-electron momentum distributions for the recollisional $(e, 2e)$ process in NSDI of He in 45-fs linearly polarized laser pulses at 800 nm [8]. According to the rescattering model, the highest energy of the laser-induced returning electron is $3.17U_p$. For the peak laser intensity used in the experiment, which is claimed to be 4.5×10^{14} W/cm^2, the maximum incident energy is 86 eV.

Following the numerical procedures presented in Sec. II(B), we first calculate the momentum distributions for two outgoing electrons in the laser-free $(e, 2e)$ process on He^+ by using the 2C, 3C, 4C, DS3C, and DS4C models, and the results for incident energies of 60, 65, and 70 eV are displayed in Fig. 2, in which the momentum components are along the incident direction, which is taken to be $+\hat{z}$. First of all, one can see that without taking into account the final-state e-e repulsion, the 2C model fails to reproduce the fingerlike structure. In contrast, including the postcollision Coulomb interaction between the two outgoing electrons, all the theoretical models predict two fingers with increasing separation as the incident energy increases. This is due to the fact the Coulomb repulsion between the two outgoing electrons prevent them from approaching each other. The comparison between those calculations including and excluding the final-state e-e repulsion clearly demonstrates that the final-state e-e repulsion plays a vital role in the formation of the two-finger structural momentum distribution. Comparing the results of the 3C model with those of the 4C model, one can see that including the precollision Coulomb interaction between the incident electron and the target ion increases the length of the two fingers. In the meantime, the two fingers change the orientation such that the momentum distributions exhibit a transition from V-type to line-shaped structure parallel to the diagonal. On the other hand, although it has been demonstrated that the dynamic screening effect plays an important role in the process of electron impact ionization of atoms at low incident energies [17,18], for the $(e, 2e)$ process on ions the dynamic screening effect becomes weaker since the charge of the residual ion becomes two times larger and thus the relative changes of the Sommerfeld parameters due to dynamic screening are smaller. The dynamic screening effect in the $(e, 2e)$ process on He^+ can be seen by comparing the DS3C model with the 3C model and comparing the DS4C model with the 4C model. While DS3C produces slightly more distributions between the two fingers compared to 3C, the main pattern from DS4C almost remains the same as that from 4C.

With the well-prepared momentum distributions for the two outgoing electrons in the laser-free $(e, 2e)$ process on He^+ at all possible incident energies, the correlated two-electron momentum spectra for the laser-induced $(e, 2e)$ process in NSDI of He can be obtained by using Eq. (21). The results from the 4C model for the recollisional $(e, 2e)$ process taking place in the laser field with a wavelength of 800 nm at an intensity of 4.0×10^{14} W/cm^2 are shown in Fig. 3 for incident energies of 65, 70, and 75 eV, respectively. It should be noted that the results shown in Fig. 3 correspond to the laser-free $(e, 2e)$ processes along the incident direction $-\hat{z}$ [12]. To see the influence of the potential change due to the presence of an electric field at the instant of recollision, we take the momentum shift in Eq. (22) in the calculation of the longitudinal correlated two-electron momentum distributions in Figs. 3(a), 3(b), and 3(c), while in Figs. 3(d), 3(e), and 3(f), Eq. (26) is used for the momentum shift. It is clearly demonstrated in Fig. 3 that, when the lowering of the threshold is taken into account, the momentum distributions move to smaller momenta since the momentum shifts are reduced. Take the situation for an incident energy of 75 eV as an example; the momentum shifts in Figs. 3(c) and 3(f) are 1.86 and 1.67, respectively.

The next step in the numerical simulations is to evaluate the correlated two-electron momentum distributions for the $(e, 2e)$ process in NSDI of He in the laser field at a given intensity. For a given intensity, the recollisional $(e, 2e)$ process could

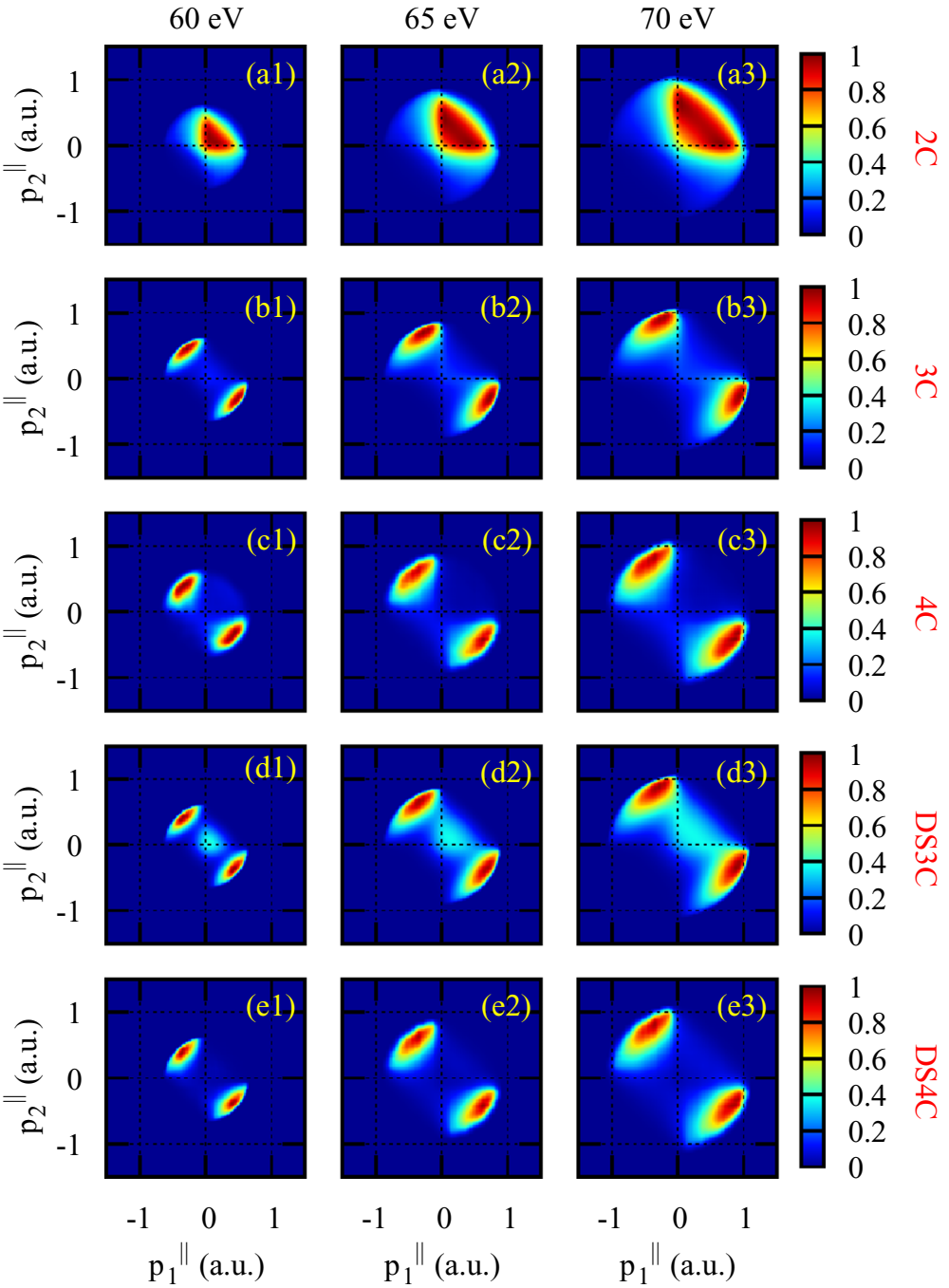

FIG. 2. Normalized momentum distributions for two outgoing electrons in the laser-free $(e, 2e)$ process on He^+ obtained by using the 2C (first row), 3C (second row), 4C (third row), DS3C (fourth row), and DS4C (fifth row) models at incident energies of 60 eV (first column), 65 eV (second column), and 70 eV (third column), respectively. Shown are the momentum components along the incident direction, which is taken to be $+\hat{z}$.

take place as long as the energy of the laser-induced electron exceeds the ionization potential. Therefore, the integration of the correlated two-electron momentum distributions over the incident energy should be performed. For this purpose, one needs to evaluate the contribution weight for the collision process at each incident energy. This weight is represented by the returning-electron wave packet, which can be calculated by using the SFA2 model [20] for HATI. In Fig. 4, we plot the wave packets against the kinetic energy of the laser-induced returning electron in 45-fs and 800-nm laser pulses at intensities of 3.0 and 4.0×10^{14} W/cm^2, respectively. Each wave packet starts with a fast drop at low energies before becoming roughly flat in the plateau region with a cutoff at $3.17U_p$. As indicated in Fig. 4, the ionization threshold of a free He^+ ion is 54.4 eV, which is lowered to 39.7 eV at the instant of recollision when the ion is exposed in the electric field at an intensity of 4.0×10^{14} W/cm^2. This indicates that, with the lowering of the threshold taken into account, more probabilities of ionization below the threshold potential of a free ion contribute to the momentum distributions.

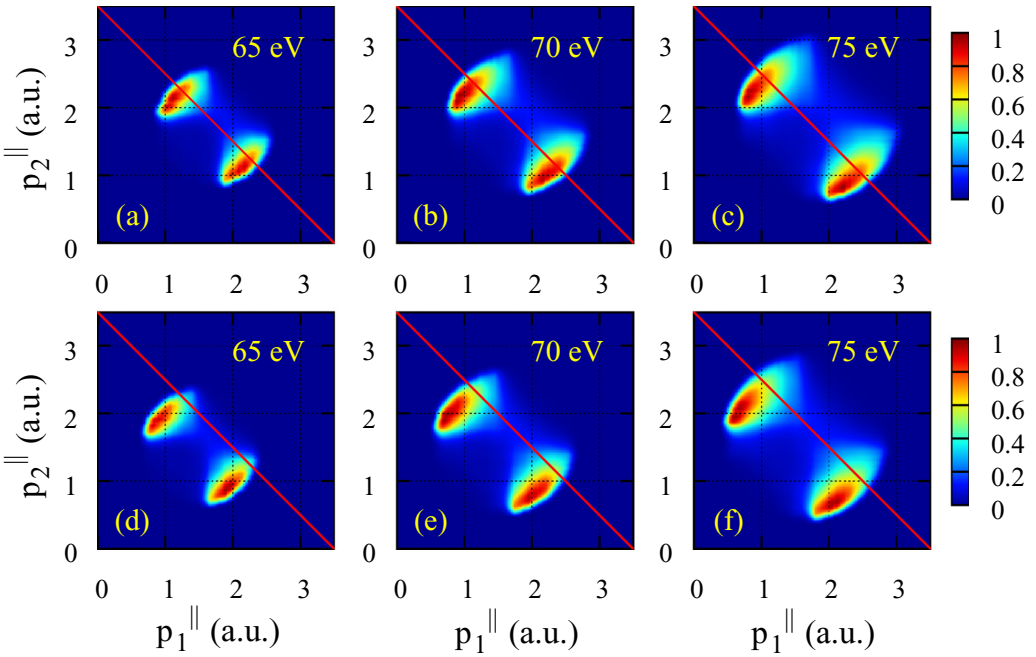

FIG. 3. Normalized momentum distributions for two outgoing electrons in the laser-induced recollisional (e, $2e$) process on He^+ at incident energies of 65, 70, and 75 eV, respectively. Lasers are at 800 nm with an intensity of 4.0×10^{14} W/cm^2. The calculated results are obtained by using the 4C model. Shown are the momentum components along the polarization direction. The potential change due to the presence of electric field at the recollision time is taken into account in panels (d), (e), and (f), but not in panels (a), (b), and (c). The red lines along the antidiagonal provide visual indication of the difference of momentum shifts between the results in the first and the second rows.

Using Eq. (27), we obtain the correlated two-electron momentum distributions for the recollisional (e, $2e$) process of He^+ in the laser field at each peak intensity. The simulated results of the 4C model are shown in Fig. 5 for laser intensities of 3.0 and 4.0×10^{14} W/cm^2, respectively; both exhibit a parallel two-finger structure with larger separation at higher intensity.

The last step in the numerical simulations is to perform the integration over the focus volume so that the obtained results can be compared with the experimental measurements directly. After focal averaging, the final correlated two-electron momentum distributions for the recollisional (e, $2e$) process in NSDI of He in 45-fs and 800-nm laser pulses at a peak intensity of 4.0×10^{14} W/cm^2 by using 2C, 3C, 4C, DS3C, and DS4C models are displayed in Fig. 6 together with the experimental measurements. The experimental data for the

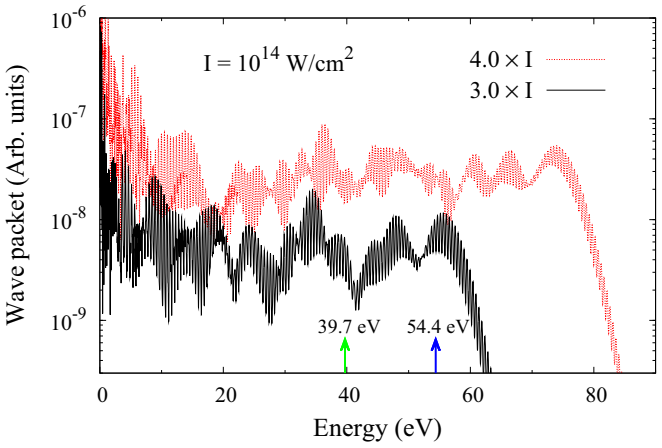

FIG. 4. Wave packets against the kinetic energy of the laser-induced returning electron in 45-fs and 800-nm laser pulses at intensities of 3.0 and 4.0×10^{14} W/cm^2, respectively. The two arrows at 39.7 and 54.4 eV indicate the ionization potential with and without taking into account the presence of the electric field at the recollision time.

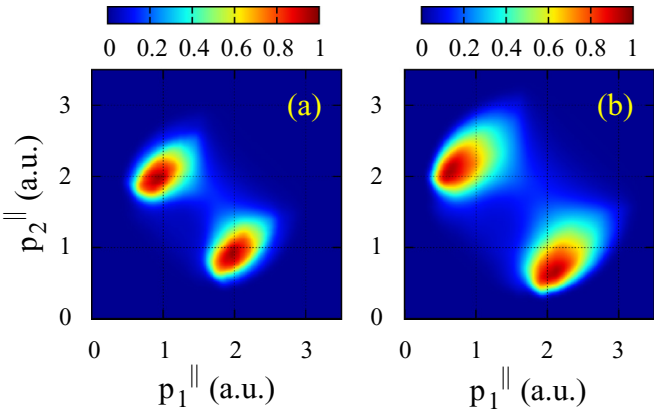

FIG. 5. Normalized momentum distributions for two outgoing electrons for the laser-induced recollisional (e, $2e$) process on He^+ in 45-fs and 800-nm pulses at the intensities of (a) 3.0×10^{14} W/cm^2 and (b) 4.0×10^{14} W/cm^2, respectively. The calculated results are obtained by using the 4C model in which the integral over all possible incident energies is performed. Shown are the momentum components along the polarization direction. The potential change due to the presence of an electric field at the recollision time is taken into account.

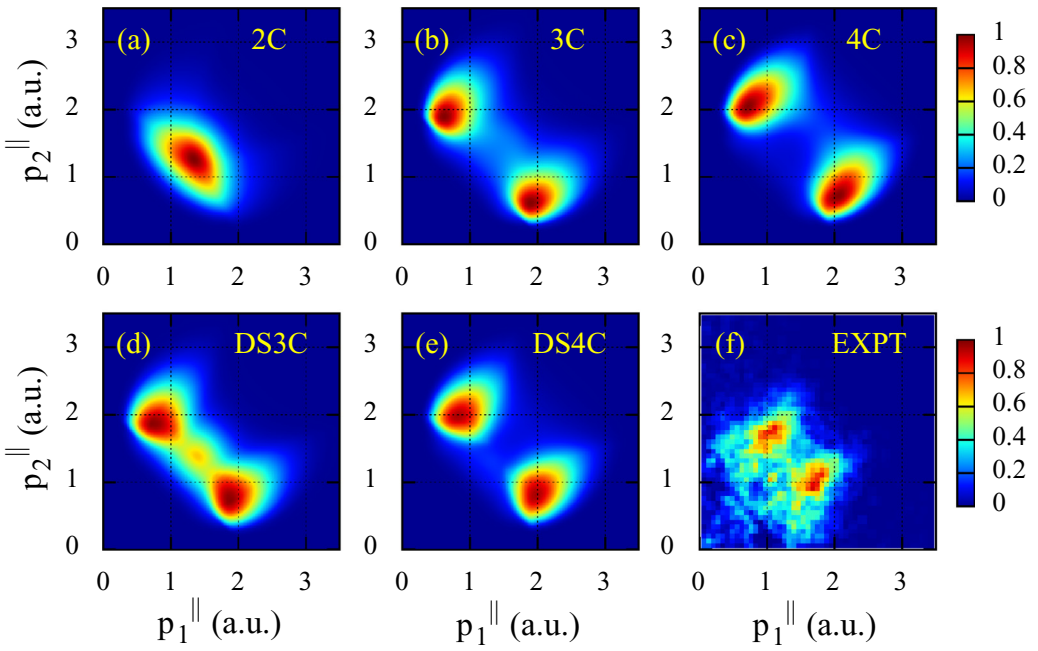

FIG. 6. Normalized correlated two-electron momentum distributions for the laser-induced recollisional $(e, 2e)$ process on He^+ in 45-fs and 800-nm laser pulses at a peak intensity of 4.0×10^{14} W/cm^2. Shown are the momentum components along the polarization direction. The potential change due to the presence of an electric field at the recollision time is taken into account, and focal volume integral is performed. The calculated results are obtained by using the theoretical models (a) 2C, (b) 3C, (c) 4C, (d) DS3C, and (e) DS4C, respectively. The experimental measurements shown in panel (f) were performed by Staudte *et al.* [8].

recollisional $(e, 2e)$ process shown in Fig. 6(f) were obtained by Chen *et al.* [11] from the original experimental data [8] based on the role of excitation tunneling in NSDI [26]. It is not surprising to see from Fig. 6 that, while the 2C model generates the momentum distributions with maximum probabilities around the diagonal, the fingerlike structure is reproduced by all the other theoretical models in which the final-state *e-e* repulsion is taken into account. Similar to the results presented in Fig. 2, including the precollision Coulomb attraction between the incident electron and the target ion, the length of the two fingers produced by the 4C model increases with different orientation with respect to the 3C model. Nevertheless, despite the very slight difference between the normalized momentum distributions of the 4C and DS4C models for each incident energy, as shown in Fig. 2, the focal-volume-averaged momentum distributions of the 4C and DS4C models displayed in Figs. 6(c) and 6(e), respectively, exhibit obvious differences. This is because the effect of dynamic screening plays a more important role in collisions at low incident energies and hence the relative contribution from collisions at low energies is enhanced. As a result, the distance between the two fingers in the DS4C model is reduced, and the agreement with the experimental measurements is improved. It is interesting to see that there exists a maximum along the diagonal in the momentum distributions of the DS3C model. This is due to the fact that in the DS3C model, the strength of the final-state *e-e* repulsion is reduced compared to that in the 3C model; consequently the two outgoing electrons have more chance to approach each other.

It should be noted that the peak intensity of the laser field used in the experimental measurements is claimed to be $(4.5 \pm 0.5) \times 10^{14}$ W/cm^2 [8]. We have carried out the numerical simulations at a few peak intensities below 4.5×10^{14} W/cm^2 and found that the simulated results at the peak intensity of 4.0×10^{14} W/cm^2 are in best agreement with the experimental results. However, some discrepancies between the simulated results and the experimental results still exist. Even the DS4C model predicts the two fingers with separation larger than what is observed in experiments. This might indicate that the final-state *e-e* repulsion is still overestimated even with the effect of dynamic screening taken into account. Interestingly, in both the quantum calculation [8] and the semiclassical simulation [9], a butterflylike structure emerges in the correlated two-electron momentum distributions, which deviates substantially from the fingerlike structure observed in experiments, indicating that the final-state *e-e* repulsion is magnified more significantly.

IV. CONCLUSIONS

Using the improved QRS model in which the potential change due to the presence of the electric field at the instant of recollision has been taken into account, we have calculated the correlated two-electron momentum distributions for the laser-induced recollisional $(e, 2e)$ process of He^+. The influences of several physical mechanisms including the final-state electron-electron and electron-nucleus interactions as well as the initial-state electron-target-ion interaction are investigated based on the full quantum mechanical level. The effects of the potential change and the dynamic screening in the final state have also been addressed. It has been found that the initial-state Coulomb interaction between the incident electron and the parent ion also plays an important role in the orientation of the two fingers and the dynamic screening reduces the

separation of the two fingers; both improve the agreement between theory and experiment. It should be emphasized that despite the slight discrepancies between the present numerical simulations and the experimental data, the DS4C model achieves the best agreement with the experimental data among all the existing theoretical results including those from *ab initio* calculations. The only deficiency of the DS4C model is that the short-range effect between the incident electron and the target ion has not been taken into account, but we believe this to be negligible for the situation considered in the present paper.

ACKNOWLEDGMENT

This work was supported by the National Natural Science Foundation of China (Grants No. 11274219 and No. 11274215).

[1] A. L'Huillier, L. A. Lompre, G. Mainfray, and C. Manus, Phys. Rev. Lett. **48**, 1814 (1982); Phys. Rev. A **27**, 2503 (1983).
[2] D. N. Fittinghoff, P. R. Bolton, B. Chang, and K. C. Kulander, Phys. Rev. Lett. **69**, 2642 (1992).
[3] B. Walker, E. Mevel, B. Yang, P. Breger, J. P. Chambaret, A. Antonetti, L. F. DiMauro, and P. Agostini, Phys. Rev. A **48**, R894 (1993).
[4] B. Walker, B. Sheehy, L. F. DiMauro, P. Agostini, K. J. Schafer, and K. C. Kulander, Phys. Rev. Lett. **73**, 1227 (1994).
[5] Y. Liu, L. Fu, D. Ye, J. Liu, M. Li, C. Wu, Q. Gong, R. Moshammer, and J. Ullrich, Phys. Rev. Lett. **112**, 013003 (2014).
[6] Z. Chen, X. Li, X. Sun, X. Hao, and J. Chen, J. Phys. B **50**, 245601 (2017).
[7] T. Weber, H. Giessen, M. Weckenbrock, G. Urbasch, A. Staudte, L. Spielberger, O. Jagutzki, V. Mergel, M. Vollmer, and R. Dorner, Nature (London) **405**, 658 (2000).
[8] A. Staudte, C. Ruiz, M. Schöffler, S. Schössler, D. Zeidler, T. Weber, M. Meckel, D. M. Villeneuve, P. B. Corkum, A. Becker, and R. Dörner, Phys. Rev. Lett. **99**, 263002 (2007).
[9] D. F. Ye, X. Liu, and J. Liu, Phys. Rev. Lett. **101**, 233003 (2008).
[10] Y. Zhou, Q. Liao, and P. Lu, Phys. Rev. A **82**, 053402 (2010).
[11] Z. Chen, Y. Liang, and C. D. Lin, Phys. Rev. Lett. **104**, 253201 (2010).
[12] Z. Chen, Y. Liang, and C. D. Lin, Phys. Rev. A **82**, 063417 (2010).
[13] Z. Chen, Y. Zheng, W. Yang, X. Song, J. Xu, L. F. DiMauro, O. Zatsarinny, K. Bartschat, T. Morishita, S. F. Zhao, and C. D. Lin, Phys. Rev. A **92**, 063427 (2015).
[14] Z. Chen, X. Li, O. Zatsarinny, K. Bartschat, and C. D. Lin, Phys. Rev. A **97**, 013425 (2018).
[15] M. Brauner, J. S. Briggs, and H. Klar, J. Phys. B **22**, 2265 (1989).
[16] J. Berakdar and J. S. Briggs, Phys. Rev. Lett. **72**, 3799 (1994).
[17] Z. Chen, Q. Shi, S. Zhang, J. Chen, and K. Xu, Phys. Rev. A **56**, R2514 (1997).
[18] Z. Chen, S. Zhang, Q. Shi, J. Chen, and K. Xu, J. Phys. B **30**, 4963 (1997).
[19] G. L. Yudin and M. Y. Ivanov, Phys. Rev. A **64**, 035401 (2001).
[20] Z. Chen, A.-T. Le, T. Morishita, and C. D. Lin, Phys. Rev. A **79**, 033409 (2009).
[21] H. W. van der Hart and K. Burnett, Phys. Rev. A **62**, 013407 (2000).
[22] E. Eremina, X. Liu, H. Rottke, W. Sandner, A. Dreischuh, F. Lindner, F. Grasbon, G. G. Paulus, H. Walther, R. Moshammer, B. Feuerstein, and J. Ullrich, J. Phys. B **36**, 3269 (2003).
[23] G. G. Paulus, W. Becker, W. Nicklich, and H. Walther, J. Phys. B **27**, L703 (1994).
[24] M. V. Ammosov, N. B. Delone, and V. P. Krainov, Zh. Eksp. Teor. Fiz. **91**, 2008 (1986).
[25] S. Augst, D. D. Meyerhofer, D. Strickland, and S. L. Chin, J. Opt. Soc. Am. B **8**, 858 (1991).
[26] B. Feuerstein, R. Moshammer, D. Fischer, A. Dorn, C. D. Schröter, J. Deipenwisch, J. R. Crespo Lopez-Urrutia, C. Höhr, P. Neumayer, J. Ullrich, H. Rottke, C. Trump, M. Wittmann, G. Korn, and W. Sandner, Phys. Rev. Lett. **87**, 043003 (2001).